JACS
JOURNAL OF THE AMERICAN CHEMICAL SOCIETY
Article
pubs.acs.org/JACS

Defining the Stoichiometry and Cargo Load of Viral and Bacterial Nanoparticles by Orbitrap Mass Spectrometry

Joost Snijder,[†,‡] Michiel van de Waterbeemd,[†,‡] Eugen Damoc,[§] Eduard Denisov,[§] Dmitry Grinfeld,[§] Antonette Bennett,[∥] Mavis Agbandje-McKenna,[∥] Alexander Makarov,[†,§] and Albert J. R. Heck*[,†,‡]

[†]Biomolecular Mass Spectrometry and Proteomics, Bijvoet Center for Biomolecular Research and Utrecht Institute for Pharmaceutical Sciences, Utrecht University, Padualaan 8, 3584 CH Utrecht, The Netherlands

[‡]Netherlands Proteomics Centre, Padualaan 8, 3584 CH Utrecht, The Netherlands

[§]Thermo Fisher Scientific (Bremen), Bremen 28199, Germany

[∥]Department of Biochemistry and Molecular Biology, Center for Structural Biology, McKnight Brain Institute, College of Medicine, University of Florida, Gainesville, Florida 32610, United States

Supporting Information

ABSTRACT: Accurate mass analysis can provide useful information on the stoichiometry and composition of protein-based particles, such as virus-like assemblies. For applications in nanotechnology and medicine, such nanoparticles are loaded with foreign cargos, making accurate mass information essential to define the cargo load. Here, we describe modifications to an Orbitrap mass spectrometer that enable high mass analysis of several virus-like nanoparticles up to 4.5 MDa in mass. This allows the accurate determination of the composition of virus-like particles. The modified instrument is utilized to determine the cargo load of bacterial encapsulin nanoparticles that were engineered to encapsulate foreign cargo proteins. We find that encapsulin packages from 8 up to 12 cargo proteins, thereby quantifying cargo load but also showing the ensemble spread. In addition, we determined the previously unknown stoichiometry of the three different splice variants of the capsid protein in adeno-associated virus (AAV) capsids, showing that symmetry is broken and assembly is heterogeneous and stochastic. These results demonstrate the potential of high-resolution mass analysis of protein-based nanoparticles, with widespread applications in chemical biology and nanotechnology.

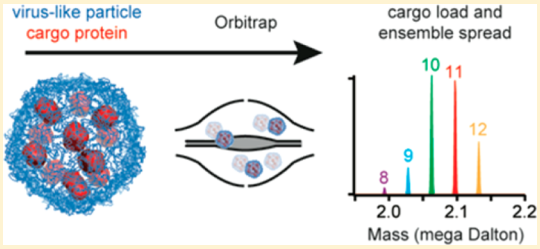

INTRODUCTION

Over the past two decades, mass spectrometry of protein complexes under near-native conditions (native MS) has developed into a field of its own.[1] Breakthroughs in instrumentation and sample preparation now make it possible to analyze intact protein complexes up to several megadaltons in mass, including membrane protein complexes, with relatively high accuracy and precision.[2−4] Our group and others have used MS to study intact virus capsids, capsid assembly, capsid composition, and cargo encapsulation.[2,5−11] There is considerable interest in the use of virus capsids for applications in vaccine delivery, gene therapy, nanomedicine, and nanotechnology.[12−16] MS analysis of these megadalton virus particles still poses a significant challenge due to reduced sensitivity of most instruments for higher masses. Native MS is traditionally and still predominantly performed on modified (quadrupole-) time-of-flight (TOF) instruments, where the operating pressures of several pumping stages are increased to improve transmission of high m/z ions via collisional cooling.[17−22] More recently, we developed an Orbitrap-based platform for application in native MS, demonstrating the use of the mass analyzer in detection of noncovalent protein complex ions up to approximately 20 000 m/z with improved resolving power compared to traditional TOF instruments modified for native MS.[23−26] It was shown that Orbitrap-based analysis offers great potential for characterizing microheterogeneity in large protein complexes, such as small ligand binding on the 800 kDa GroEL chaperonin and glycosylation profiling on intact proteins under native conditions.[23,27−30] Here, we seek to further extend and explore the upper mass limits of the Orbitrap platform with the purpose of analyzing virus like assemblies.

EXPERIMENTAL SECTION

Sample Preparation. Samples were prepared for mass spectrometry by buffer exchange to ammonium acetate, using Vivaspin 500 K 10 kDa MWCO centrifugal filter units. GroEL samples were analyzed from 50 mM ammonium acetate, pH 6.8. Encapsulin and dodecahedron samples were analyzed from 150 mM ammonium acetate, pH 6.8. The AAV1 samples were prepared as previously described[42,43] and analyzed in 100 mM ammonium acetate, pH 6.8. CCMV was analyzed from 50 mM ammonium acetate, pH 5.0. Aliquots of 1−2 μL, at a final concentration of ∼2 μM, were loaded

Received: November 28, 2013
Revised: March 14, 2014
Published: May 1, 2014

   dx.doi.org/10.1021/ja502616y | J. Am. Chem. Soc. 2014, 136, 7295−7299

into gold-coated borosilicate capillaries (prepared in-house) for nanoelectrospray ionization.

Instrument Modifications. The Exactive Plus mass spectrometer (Thermo Fisher Scientific, Bremen, Germany) was modified to include an adjustable gas supply for the HCD cell, and analogue filters were removed from the image current preamplifier to allow detection over the entire frequency range. The control software of the instrument was modified to allow the standard mass range of this instrument to be increased from m/z 50−6000 to m/z 400−40 000. In addition, maximum RF voltages were applied to all RF multipoles including the C-trap. Instead of trapping in the C-trap, ions were allowed to enter the HCD cell and were stored there prior to their return back into the C-trap. Manual tuning of the voltage offset on the transport octapole was used for mass filtering of the incoming protein ions, as previously described.[23] Frequency reduction on RF multipoles was implemented by adding high-voltage capacitors to corresponding RF coils and electronic boards automatically adjusted resonance frequency while keeping the amplitude constant.

RESULTS

On the basis of theoretical considerations regarding the ion optics of the instrument (see Supporting Information text and Figures S1 and S2), we hypothesized that more efficient focusing of ions, especially in the C-trap, would be beneficial for transmission of high m/z ions (>20 000). A schematic of the instrument is presented in Figure 1. We sought to more

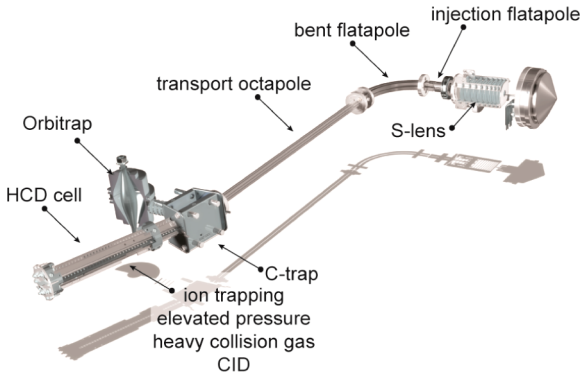

Figure 1. Schematic of the Exactive Plus instrument.

effectively focus high mass ions in the front-end ion guides and C-trap by lowering their RF frequency. The effects of reducing the RF frequencies of the front-end ion guides on high m/z ion transmission were tested on large Cesium Iodide clusters (up to 20 000 m/z) and GroEL CID product ions (ranging from 15 000 to 40 000 m/z). A 5- to 10-fold increase in ion transmission could be demonstrated for CsI clusters at 20 000 m/z and GroEL product ions at 30 000 m/z. Moreover, the instrument modifications allowed detection of GroEL product ions up to 40 000 m/z, compared to 30 000 m/z in the standard configuration. At the transient time of 64 ms that was used to analyze GroEL, intact 14-mer ions are detected with an effective resolution of ∼1500 ($M/\Delta M$, fwhm), whereas there is a shallow decline in effective resolution for the higher m/z 13-mer and 12-mer ions, down to ∼1000 at m/z 40 000 (see Supporting Information Table S1 and Figures S3−S5).

We further explored the performance of the modified instrument for the analysis of megadalton (MDa) virus assemblies (Figure 2). Therefore, we analyzed an array of particles, namely the bacterial nanocontainer encapsulin (2.1 MDa, d ∼ 24 nm), the adenovirus dodecahedron (Dd, 3.5 MDa, d ∼ 22 nm), adeno-associated virus serotype 1 (AAV1,

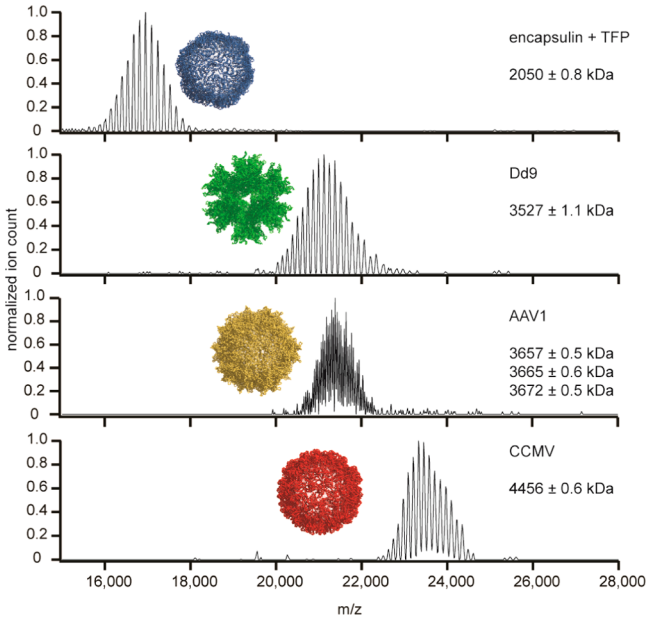

Figure 2. Native MS of virus-like particles on the modified Exactive Plus. Shown are encapsulin (top), adenovirus dodecahedron (top-middle), adeno-associated virus serotype 1 (bottom-middle) and cowpea chlorotic mottle virus (bottom). Corresponding structures are also shown on the graphs. The quoted masses represent the average ± standard deviation over all charge states in the spectrum. For detailed peak assignments, see Supporting Information Table S2.

3.7 MDa, d ∼ 27 nm), and cowpea chlorotic mottle virus (CCMV, 4.5 MDa, d ∼ 28 nm). Encapsulin, Dd, AAV1, and CCMV could all be mass analyzed on the modified instrument (see Figure 2). All the detected ion signals originate from well-defined charge state distributions that are nearly baseline resolved for all species. The standard deviations on the obtained masses are all on the order of 0.01%. Details of the peak assignments are provided in Supporting Information Table S2. These MS analyses are considerably more precise and accurate than conventional techniques that are used to determine the size and mass of protein nanoparticles, such as size exclusion chromatography, light-scattering based techniques or gel-based assays. Although attempted, we were so far not able to analyze particles larger than CCMV, such as the 13 MDa HK97 head II particle on the Orbitrap-based platform.[31] It is estimated that the upper limit of the instrument for intact protein complexes is currently at 25 000−30 000 m/z, corresponding to a mass of roughly 5 MDa in positive-mode nanoelectrospray. Because all ions generated in the source must pass the C-trap twice, which we identified as a bottleneck for high-mass transmission, this limit is lower compared to the highest m/z that can be observed for HCD product ions, which only pass the C-trap once after being generated in the HCD cell.

Encapsulin is a recently discovered bacterial nanoparticle, consisting of 60 copies of a capsid-like protein that form a $T = 1$ icosohedral capsid-like particle that encapsulates a functional enzyme in vivo in bacteria.[32] More recently, it was shown that encapsulin can also be utilized as a nanocontainer to package non-native cargo proteins.[33] To demonstrate the utility of the modified Orbitrap platform in chemical biology and nanotechnology, we analyzed encapsulin loaded with foreign fluorescent cargo proteins (Figure 3). Whereas the spectrum in Figure 2 seems to represent a single charge state distribution,

dx.doi.org/10.1021/ja502616y | J. Am. Chem. Soc. 2014, 136, 7295−7299

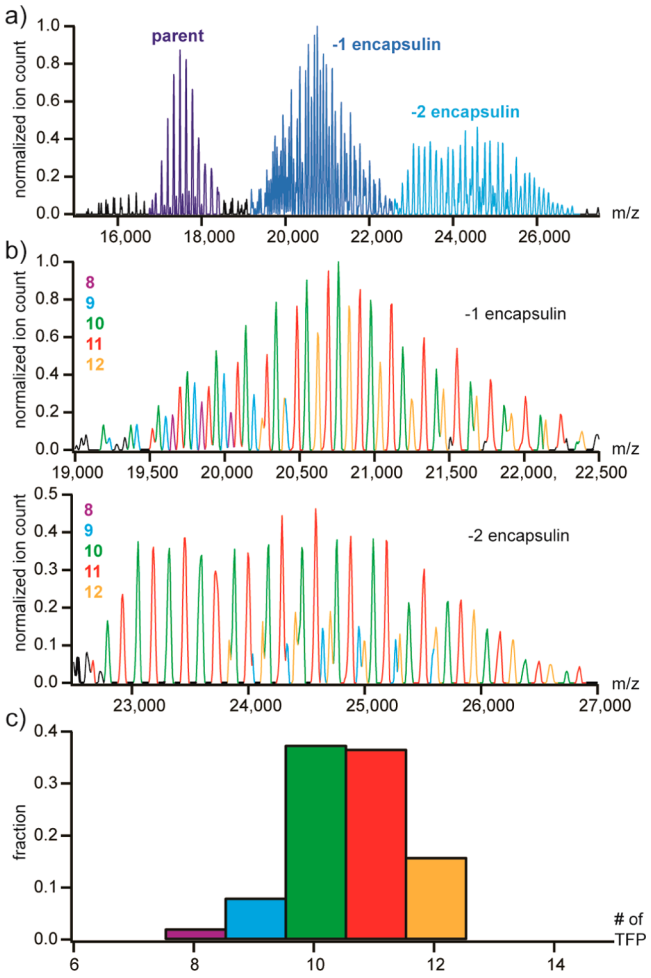

Figure 3. Identifying and quantifying foreign cargo encapsulation (Teal Fluorescent Protein, TFP) in bacterial encapsulin. (a) Native MS spectrum of encapsulin at high collision energy, showing dissociation of up to two encapsulin monomeric subunits. (b) Zoom-in of the peaks corresponding to the first (top) and second (bottom) dissociation products; colors according to number of encapsulated cargo molecules. (c) Total intensity of all identified encapsulin-cargo stoichiometries. For detailed peak assignments, see Supporting Information Table S3.

we observed that it is actually the sum of many very closely overlapping distributions, originating from the encapsulin nanoparticle with a variable number of the cargo proteins encapsulated. We discovered this only when we applied high energy to the ions in the HCD cell, promoting dissociation, whereby subsequently up to two encapsulin monomeric subunits became expelled from the intact precursor ions. In the resulting high m/z fragment ions, the underlying distributions of the different species became resolved (Figure 3).

The resulting masses correspond to an integer number of loaded cargo proteins, thereby verifying the more accurate mass assignments on the HCD product ions compared to the intact parent ions (see Supporting Information Table S3). We observe charge state distributions corresponding to nanoparticles of the 60-mer encapsulin, encapsulating between exactly 8 and 12 copies of foreign fluorescent cargo molecule. The intensity weighted average number of encapsulated cargo molecules is determined at 10.6 TFP per encapsulin nanoparticle. The results show that the modified Orbitrap platform can be used to quantify the encapsulated cargo in this ~2 MDa bacterial nanocontainer with sufficient resolution to also characterize the ensemble spread. To validate the above quantitation procedure, we used the extracted intensity information on the individual encapsulin-cargo stoichiometries to reconstruct a theoretical spectrum for the intact particle (Supporting Information Figure S6). We used an in-house developed software package SOMMS (SOlving complex Macromolecular Mass Spectra) to generate spectra of encapsulin 60-mer with 8−12 copies of the cargo molecule.[34] These spectra illustrate how the very close overlap between the different charge state distributions results in one unresolved ion series (the required resolution to separate these peaks at half-height is 2500−3000, currently beyond the capabilities of the instrument). Summing the theoretical spectra together reasonably reproduces the experimental spectrum of the undissociated encapsulin with the determined mixed number of fluorescent cargo proteins encapsulated.

The Dd and AAV1 particles have similar masses of around 3.5 MDa. Still, the corresponding mass spectra shown in Figure 2 look strikingly different. Dd has been proposed as a noninfective vector for gene transfer and is structurally a dodecahedron made of adenovirus pentons, i.e., a 60-mer homo-oligomeric assembly, having a single defined mass. AAV1 has a $T = 1$ icosahedral capsid and is extensively used as a vector for gene therapy and vaccine delivery.[35,36] It is the first approved gene therapy vector in the Western world.[37] In AAVs, alternatively splicing and differential codon usage of a single capsid gene produces three variants of the capsid viral protein, VP1/VP2/VP3. The VP3 sequence is common between all three splice variants, and VP2 and VP1 have N-terminal longer sequences, with VP1 containing a phospholipase domain in its unique region. The exact amounts of VP1/VP2/VP3 in the capsid are unknown but estimated to be 1/1/10, based on densitometry analyses of the capsid proteins resolved on SDS-PAGE.[38−40] Despite many reported crystal structures and cryo-electron microscopy reconstructions of several AAV serotypes, it is currently not known whether there is any defined VP1/VP2/VP3 stoichiometry in the capsid, as only the common part between the three splice variants (VP3) is clearly resolved in those structures. In our mass spectrum of AAV1 capsids, we were able to resolve three series of peaks (see Figure 4). From the calculated masses, we can determine the copy numbers of VP1/VP2/VP3, also applying the constraint that the total copy number in the capsid is fixed at $n = 60$. On the basis of the sequences of VP1/VP2/VP3, their monomer masses are calculated to be 81375/66225/59606 Da, respectively. On the basis of these theoretical masses, the experimental masses of the intact capsids were used to estimate the VP1/VP2/VP3 copy numbers, where we considered every theoretical mass within 2 standard deviations of the experimental mass to be a possible match.

The masses listed in Figure 4 correspond to capsids with a single copy of VP1 and between 9 and 11 copies of VP2 (with all remaining subunits VP3). For all three series of peaks, the charge state assignment is relatively ambiguous. We get a similar standard deviation of 0.5 kDa on the calculated masses, regardless of whether the masses are calculated using the charge-state range of 165−178 or 164−177 (a bigger shift in charge state assignment does result in bigger errors). By simulating theoretical spectra of AAV1 capsids with different VP1/VP2/VP3 stoichiometries using SOMMS, it became apparent that there is substantial peak overlap between capsids

dx.doi.org/10.1021/ja502616y | J. Am. Chem. Soc. 2014, 136, 7295−7299

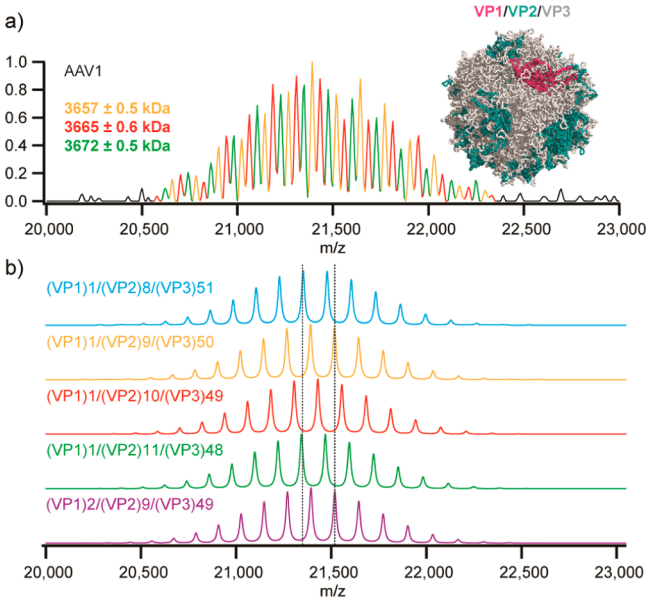

Figure 4. Determining the VP1/VP2/VP3 stoichiometry in AAV1. (a) Experimental spectrum of AAV1 capsids recorded at 32 ms transient time. The AAV1 capsid structure is shown with scattered copies of VP1/VP2. (b) Simulated spectra of AAV1 capsids with different VP1/VP2/VP3 stoichiometries. The simulated spectra illustrate how there is partial overlap between peaks of capsids with different VP1 and VP2 copy numbers.

with different VP1 and VP2 copy numbers and that it is therefore fundamentally impossible to resolve more than the three series of peaks (Figure 4b). Considering the two alternative charge state assignments, we calculated a total of six masses, matching a total of 8 stoichiometries (see Supporting Information Table S4). From these calculations, we extract that there are 0−2 copies of VP1, 8−11 copies of VP2, and 48−51 copies of VP3 in individual AAV1 particles. These results demonstrate for the first time that there is no defined VP1/VP2/VP3 stoichiometry for AAV1 and, therefore, suggest that assembly is stochastic such that the relative amount of VP1/VP2/VP3 that is incorporated in the capsid might depend mainly on their relative expression levels. The variable copy numbers of VP1/VP2/VP3 offer an explanation for the lack of VP1/VP2 density in the structural analyses of AAV, as the lack of symmetry would preclude VP1/VP2 to clearly appear in reconstructions of the particles.

To illustrate the benefit of the native MS-based approach described here, data acquired by SDS-PAGE and negative stain electron microscopy on AAV1 particles are provided in Supporting Information Figure S7. These represent more conventional techniques for the analysis of AAV and other protein-based nanoparticles in general. Whereas SDS-PAGE does provide good separation of VP1/VP2/VP3, such an experiment only provides an ensemble average regarding the relative amounts of the three different capsid proteins, as the particles fully disassemble when analyzed under denaturing conditions. Techniques such as negative stain electron microscopy visualize the intact particles, but despite the relatively high spatial resolution attained, no information can be gained on the relative amounts of VP1/2/3 in the absence of any distinct morphological features. SEC or gel shift assays similarly lack the resolution to resolve mass differences on the order of 0.1%. As discussed above, even when the particles were analyzed with atomic-level resolution using X-ray crystallography, no density corresponding to the unique regions of VP1 and VP2 could be seen, because of the inherent variability between the particles. For these reasons, the ability to determine with high precision and mass resolving power the absolute masses of nanoparticles makes the MS-based approach described here a uniquely powerful analytical tool.

DISCUSSION

Most native MS platforms described so far employ a markedly different strategy for improving transmission of high mass ions. In most TOF-based platforms, the source regions and ion guides are operated at elevated pressure to improve transmission of high mass ions via collisional cooling.[17−22] Whereas enhanced collisional cooling is in principle also possible on the Orbitrap-based instrument described here, there is a possible benefit of the strategy for improved high mass transmission that we employ. By increasing the quasi-potential well depth of the ion focusing devices, we prevent the introduction of excessive gas in regions of the instruments where this is unwanted. Most notably, it was recently demonstrated that the main reason for a decay of signal for larger ions in the analyzer is due to collisions with background gas.[41] We identified the C-trap as a bottleneck for efficient high mass transmission, but collisional cooling in this region would lead to particularly high pressures in the Orbitrap as well, which we anticipate to lead to rapid decay of coherent and stable oscillation of the ions inside the Orbitrap analyzer.

In conclusion, we have identified limitations for high mass analysis in the Orbitrap-based platform for native MS and developed a successful strategy to improve the instruments sensitivity at high m/z. This allows the characterization of virus-like assemblies with superior mass resolving power, thereby facilitating analyses such as the quantification of cargo encapsulation in engineered virus like particles for nanotechnology, and the precise definition of protein stoichiometries in heterogeneous protein assemblies.

ASSOCIATED CONTENT

Supporting Information

Supplementary text, experimental procedures, and Tables S1−S4 and Figures S1−S7. This material is available free of charge via the Internet at http://pubs.acs.org.

AUTHOR INFORMATION

Corresponding Author

a.j.r.heck@uu.nl

Notes

The authors declare the following competing financial interest(s): See text;Eu.D.,Ed.D., D.G. and A.M. are employees of Thermo Fisher Scientific Inc., the company that produces and sells the Exactive Plus EMR instrument.

ACKNOWLEDGMENTS

We kindly acknowledge our collaborators for providing the virus and encapsulin samples. Encapsulin and CCMV samples were provided by W. F. Rurup, M. Brasch, M. S. T Koay and J. J. L. M. Cornelissen (MESA+ Institute for Nanotechnology, University of Twente, The Netherlands). Adenovirus dodecahedron samples were provided by E. Szolajska and J. Chrobozcek (IBB, Polish Academy of Sciences, Poland). J.S., M.vd.W. and A.J.R.H are supported by The Netherlands

Proteomics Centre. M.vd.W. and A.J.R.H. are additionally supported by a Projectruimte grant (12PR3303-2) from Fundamenteel Onderzoek der Materie (FOM). A.B. and M.A.-M. are supported by NIH R01 GM109524 and funds from the UF College of Medicine.

REFERENCES

(1) Sharon, M. *Science* **2013**, *340*, 1059−1060.
(2) Snijder, J.; Rose, R. J.; Veesler, D.; Johnson, J. E.; Heck, A. J. R. *Angew. Chem., Int. Ed.* **2013**, *52*, 4020−4023.
(3) Laganowsky, A.; Reading, E.; Hopper, J. T. S.; Robinson, C. V. *Nat. Protoc.* **2013**, *8*, 639−651.
(4) Morgner, N.; Montenegro, F.; Barrera, N. P.; Robinson, C. V. *J. Mol. Biol.* **2012**, *423*, 1−13.
(5) Uetrecht, C.; Barbu, I. M.; Shoemaker, G. K.; Van Duijn, E.; Heck, A. J. R. *Nat. Chem.* **2011**, *3*, 126−132.
(6) Snijder, J.; Uetrecht, C.; Rose, R. J.; Sanchez-Eugenia, R.; Marti, G. A.; Agirre, J.; Guérin, D. M. A.; Wuite, G. J. L.; Heck, A. J. R.; Roos, W. H. *Nat. Chem.* **2013**, *5*, 502−509.
(7) Brasch, M.; De La Escosura, A.; Ma, Y.; Uetrecht, C.; Heck, A. J. R.; Torres, T.; Cornelissen, J. J. L. M. *J. Am. Chem. Soc.* **2011**, *133*, 6878−6881.
(8) Fuerstenau, S. D.; Benner, W. H.; Thomas, J. J.; Brugidou, C.; Bothner, B.; Siuzdak, G. *Angew. Chem., Int. Ed.* **2001**, *40*, 542−544.
(9) Tito, M. A.; Tars, K.; Valegard, K.; Hajdu, J.; Robinson, C. V. *J. Am. Chem. Soc.* **2000**, *122*, 3550−3551.
(10) Keifer, D. Z.; Pierson, E. E.; Hogan, J. A.; Bedwell, G. J.; Prevelige, P. E.; Jarrold, M. F. *Rapid Commun. Mass Spectrom.* **2014**, *28*, 483−488.
(11) Pierson, E. E.; Keifer, D. Z.; Selzer, L.; Lee, L. S.; Contino, N. C.; Wang, J. C. -.; Zlotnick, A.; Jarrold, M. F. *J. Am. Chem. Soc.* **2014**, *136*, 3536−3541.
(12) O'Neil, A.; Reichhardt, C.; Johnson, B.; Prevelige, P. E.; Douglas, T. *Angew. Chem., Int. Ed.* **2011**, *50*, 7425−7428.
(13) Patterson, D. P.; Prevelige, P. E.; Douglas, T. *ACS Nano* **2012**, *6*, 5000−5009.
(14) Wörsdörfer, B.; Woycechowsky, K. J.; Hilvert, D. *Science* **2011**, *331*, 589−592.
(15) Vriezema, D. M.; Aragonès, M. C.; Elemans, J. A. A. W.; Cornelissen, J. J. L. M.; Rowan, A. E.; Nolte, R. J. M. *Chem. Rev.* **2005**, *105*, 1445−1489.
(16) Comellas-Aragonès, M.; Engelkamp, H.; Claessen, V. I.; Sommerdijk, N. A. J. M.; Rowan, A. E.; Christianen, P. C. M.; Maan, J. C.; Verduin, B. J. M.; Cornelissen, J. J. L. M.; Nolte, R. J. M. *Nat. Nanotechnol.* **2007**, *2*, 635−639.
(17) Benesch, J. L. P.; Ruotolo, B. T.; Sobott, F.; Wildgoose, J.; Gilbert, A.; Bateman, R.; Robinson, C. V. *Anal. Chem.* **2009**, *81*, 1270−1274.
(18) Chernushevich, I. V.; Thomson, B. A. *Anal. Chem.* **2004**, *76*, 1754−1760.
(19) Kozlovski, V. I.; Donald, L. J.; Collado, V. M.; Spicer, V.; Loboda, A. V.; Chernushevich, I. V.; Ens, W.; Standing, K. G. *Int. J. Mass Spectrom.* **2011**, *308*, 118−125.
(20) Krutchinsky, A. N.; Chernushevich, I. V.; Spicer, V. L.; Ens, W.; Standing, K. G. *J. Am. Soc. Mass Spectrom.* **1998**, *9*, 569−579.
(21) Sobott, F.; Hernández, H.; McCammon, M. G.; Tito, M. A.; Robinson, C. V. *Anal. Chem.* **2002**, *74*, 1402−1407.
(22) Van Den Heuvel, R. H. H.; Van Duijn, E.; Mazon, H.; Synowsky, S. A.; Lorenzen, K.; Versluis, C.; Brouns, S. J. J.; Langridge, D.; Van Der Oost, J.; Hoyes, J.; Heck, A. J. R. *Anal. Chem.* **2006**, *78*, 7473−7483.
(23) Rose, R. J.; Damoc, E.; Denisov, E.; Makarov, A.; Heck, A. J. R. *Nat. Methods* **2012**, *9*, 1084−1086.
(24) Makarov, A. *Anal. Chem.* **2000**, *72*, 1156−1162.
(25) Zubarev, R. A.; Makarov, A. *Anal. Chem.* **2013**, *85*, 5288−5296.
(26) Belov, M. E.; Damoc, E.; Denisov, E.; Compton, P. D.; Horning, S.; Makarov, A. A.; Kelleher, N. L. *Anal. Chem.* **2013**, *85*, 11163−11173.
(27) Rosati, S.; van den Bremer, E. T.; Schuurman, J.; Parren, P. W.; Kamerling, J. P.; Heck, A. J. *MAbs* **2013**, *5*, 917−924.
(28) Rosati, S.; Rose, R. J.; Thompson, N. J.; van Duijn, E.; Damoc, E.; Denisov, E.; Makarov, A.; Heck, A. J. *Angew. Chem., Int. Ed.* **2012**, *51*, 12992−12996.
(29) Yang, Y.; Barendregt, A.; Kamerling, J. P.; Heck, A. J. *Anal. Chem.* **2013**, *85*, 12037−12045.
(30) Thompson, N. J.; Hendriks, L. J. A.; de Kruif, J.; Throsby, M.; Heck, A. J. R. *MAbs* **2014**, *6*, 197−203.
(31) Veesler, D.; Khayat, R.; Krishnamurthy, S.; Snijder, J.; Huang, R.; Heck, A. R.; Anand, G.; Johnson, J. *Structure* **2013**, *22*, 230−237.
(32) Sutter, M.; Boehringer, D.; Gutmann, S.; Günther, S.; Prangishvili, D.; Loessner, M. J.; Stetter, K. O.; Weber-Ban, E.; Ban, N. *Nat. Struct. Mol. Biol.* **2008**, *15*, 939−947.
(33) Rurup, W. F.; Snijder, J.; Koay, M. S. T.; Heck, A. J. R.; Cornelissen, J. J. L. M. *J. Am. Chem. Soc.* **2014**, *136*, 3828−3832.
(34) Van Breukelen, B.; Barendregt, A.; Heck, A. J. R.; Van Den Heuvel, R. H. H. *Rapid Commun. Mass Spectrom.* **2006**, *20*, 2490−2496.
(35) Agbandje-McKenna, M.; Kleinschmidt, J. *Methods Mol. Biol.* **2011**, *807*, 47−92.
(36) Mingozzi, F.; High, K. A. *Nat. Rev. Genet.* **2011**, *12*, 341−355.
(37) Melchiorri, D.; Pani, L.; Gasparini, P.; Cossu, G.; Ancans, J.; Borg, J. J.; Drai, C.; Fiedor, P.; Flory, E.; Hudson, I.; Leufkens, H. G.; Müller-Berghaus, J.; Narayanan, G.; Neugebauer, B.; Pokrotnieks, J.; Robert, J. -.; Salmonson, T.; Schneider, C. K. *Nat. Rev. Drug Discovery* **2013**, *12*, 719.
(38) Rose, J. A.; Maizel, J. V., Jr.; Inman, J. K.; Shatkin, A. J. *J. Virol.* **1971**, *8*, 766−770.
(39) Buller, R. M.; Rose, J. A. *J. Virol.* **1978**, *25*, 331−338.
(40) Johnson, F. B.; Ozer, H. L.; Hoggan, M. D. *J. Virol.* **1971**, *8*, 860−863.
(41) Makarov, A.; Denisov, E. *J. Am. Soc. Mass Spectrom.* **2009**, *20*, 1486−1495.
(42) Miller, E. B.; Gurda-Whitaker, B.; Govindasamy, L.; McKenna, R.; Zolotukhin, S.; Muzyczka, N.; Agbandje-McKenna, M. *Acta Crystallogr., Sect. F: Struct. Biol. Cryst. Commun.* **2006**, *62*, 1271−1274.
(43) Zolotukhin, S.; Potter, M.; Zolotukhin, I.; Sakai, Y.; Loiler, S.; Fraites, T. J., Jr.; Chiodo, V. A.; Phillipsberg, T.; Muzyczka, N.; Hauswirth, W. W.; Flotte, T. R.; Byrne, B. J.; Snyder, R. O. *Methods* **2002**, *28*, 158−167.